Design of Bidirectional Converter for Wireless EV Charging System

D.Sravani[1], K.Divya[2], P. Lakshmi Madhuri[3],G.Lokesh[4], M.Tarakeswara Rao[5],B.Lakshmana[6], Amaleswari Rajulapati[7]

[1,2,3,4,5,6]Departmentof EEE / UG Student, NSRIT(A), Visakhapatnam, Andhra Pradesh, India
[7]Department of EEE / Associate Professor, NSRIT(A), Visakhapatnam, Andhra Pradesh, India
(rajulapatiamaleswari2022@gmail.com, 22NU1A0209@nsrit.edu.in)

Corresponding Author; Amaleswari Rajulapati, Associate Professor, Nadimpalli Satyanarayana Raju Institute of Technology (Autonomous), Sontyam, Visakhapatnam, Andhra Pradesh, India – 531173., Tel: +91 9884489614, rajulapatiamaleswari2022@gmail.com

ABSTRACT

In this work, a dual active bridge-based non-contact isolated bidirectional symmetrical resonant converter is suggested as the primary structure. An isolated bidirectional symmetrical resonant conversion circuit is created by integrating this technique with the symmetrical resonant network. This work uses the symmetrical resonance technique to decrease the power loss and electromagnetic noise caused by hard switching of power switches in the circuit, improve overall converter efficiency, voltage regulation, and hard switching from conventional bidirectional converters, and realise the function of soft switching and voltage regulation of a wide range of output under the proper operating frequency. Additionally, the traditional transformer is replaced with a pair of non-contact loosely connected inducers (wireless coils) to wirelessly transmit the bidirectional energy. The EV battery side is set to 670–800 V, while the suggested converter's DC grid input voltage is set to 400 V. The bidirectional wireless charger has a 2 kW rated power capacity. In addition, the CC-CV charging feature of the suggested bidirectional wireless EV charger satisfies the EV charging criteria. Lastly, forward charging mode (grid to vehicle [G2V; 400 V charge to 800 V]) may achieve a maximum efficiency of 90.2%, while reverse discharging mode (vehicle to grid [V2G; 800 V discharge to 400 V]) can achieve 91.4%.

KEYWORDS: Wireless Charging EV, Bidirectional Converter, Electric Vehicle

I. INTRODUCTION

Human needs for diverse technological resources have grown in order to expand and enhance technology, but the effects of scientific and technological advancements on the environment have also increased. Therefore, to lessen reliance on conventional energy sources and their negative effects on the environment, renewable energy must be developed and used. Conversion and use of natural resources, including wind, solar, and water power, are the most prevalent forms of renewable energy [1], [2]. However, because renewable energy is usually influenced by seasonal and meteorological conditions, electricity generation is highly unreliable. An inadequate power supply will result from this instability issue. surplus electricity output during off-peak hours and peak power usage.As a result, energy conversion is crucial to the evolution of renewable energy and storage [3]. Since a converter device is necessary for energy storage and battery discharge, the entire system exhibits the drawbacks of size and expense due to the need for numerous sets of converters. The whole system may stabilise through its bidirectional power transmission structure, increase the efficiency of the entire converter, and maximise the rate of energy utilisation if a bidirectional converter [4], [5] can be utilised in lieu of the conventional structure. The energy storage and release idea [6], which integrates a two-way energy storage system with renewable energy, Batteries and energy storage are the two main applications for DC power sources. The primary research structure in this work is represented by the green-dotted block. A DC/DC converter is attached to the post-stage of PV, wind and hydroelectricity to raise the output DC level to 400 VtoDC grid.The EV battery may then be charged to 800 V using the EVBi-directional charger. These days, EV batteries have a voltage of 800 V for a number of benefits [10].The first is that, at the same charging power level, the 800V EV battery takes nearly half as long to charge as the 400V EV battery. The second is that an 800V battery has a higher charging current than a 400V battery.It implies that while charging an 800V EV battery, the charging cable's diameter might be reduced. Put otherwise, an 800VEV cable can save more money with a lower charging current.For resonant converters, the LLC topology is frequently used [11] and [12].

II. ANALYSIS OF THE PROPOSED CONVERTER

A. PROPOSE CONVERTER CONFIGURATION

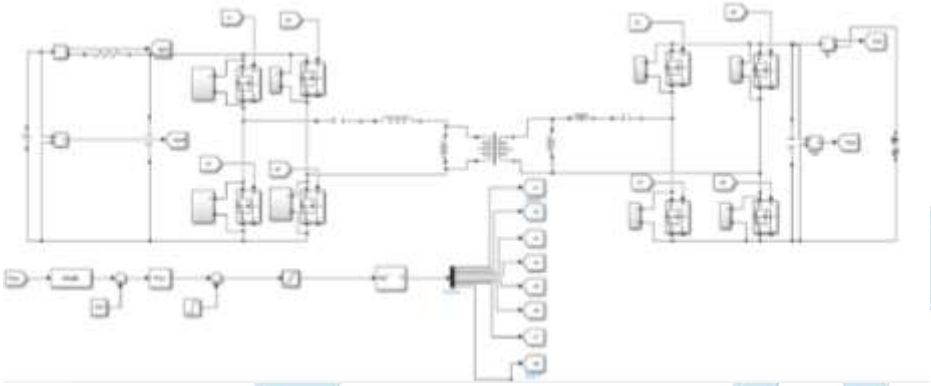

This paper proposes and implements an isolated bidirectional symmetrical resonant converter. In 2, the circuit structure is displayed. The grid port that provides electricity to the battery's energy storage and discharge port is known as the forward charging mode. In the meanwhile, the battery port that provides electricity to the grid port is known as the reverse discharge mode. This circuit shares many of the same properties as a bidirectional LLC resonant converter. On the secondary side of the conventional LLC resonant circuit transformer, rectifier switches are used in place of rectifier diodes, and a resonant element is added on the load side. how two-way energy transfer works.

Fig. 3 shows the voltage gain curve based on the bidirectional resonant converter's design parameters as determined by the mathematical operation simulation program Mathcad. The full-bridge resonant converter uses a symmetrical resonance parameter design to guarantee that the forward and reverse voltage gain curves are comparable, as seen by the gain curve in the forward charging mode operation. Based on the resonant frequency (fr), its gain may be separated into three intervals and fluctuates with the switching frequency.

B. OPERATION PRINCIPLES

In order to guarantee that the power switches may accomplish zero-voltage switching function in bidirectional circuit operation, the symmetric resonant circuit in this work exhibits the properties of soft switching. when the converter is functioning within the proper resonance range. In the meantime, the secondary side rectifier switch's zero-current switching effect may significantly lower power loss and successfully raise the circuit's total conversion efficiency. The theoretical waveform of the converter operating in Region II is displayed in Fig. 4, and operating stages I through VI will introduce its working principle. Since the principles of operation of the positive and negative half cycles are identical, the study uses the six modes of the positive half cycle as an example.

1) OPERATION STAGE 1 ($t_o < t \leq t_1$)

While power switches S1 and S4 stay off and the circuit enters dead time at t = t0, gate signals vGS2 and vGS3 of power switches S2 and S3 transition from the on state to the off state, as seen in Fig. 5. The power switch's parasitic capacitances Coss1 and Coss4 release energy through iLr1, while iLr1 stores energy for Coss2 and Coss3. The resonant current iLr1 keeps the current flowing in the same direction. Furthermore, because ir1 and iLm are not equal, the current difference rectifies the output through body diodes DB5 and DB8 and sends energy to the secondary side via the wireless coils.When the power switch's parasitic capacitances Coss1 and Coss4 are fully discharged to zero and Coss2 and Coss3 are charged to VGrid, this operating stage comes to an end.

2) OPERATING STAGE 2 ($t_1 < t \leq t_2$)

When t = t1, power switches S1 through S4 are all off, as seen in Fig. 6. Through the power switch's body diodes DB1 and DB4, the resonant current iLr1 creates a freewheeling state, ensuring that power switches S1 and S4 provide the zero-voltage switching condition. When S1 and S4 are activated, the zero-voltage switching function is realised. iLr1 is still supplying energy to the secondary side at this moment, enabling diodes DB5 and DB8 to conduct. When t = t2, the operating stage comes to a close. Gate signals vGS1 and vGS4 of power switches S1 and S4 transition from the off state to the on state.

3) OPERATING STAGE 3($t_3 < t \leq t_4$)

When t = t2, as seen in Fig. 7, S1 and S4 are activated, and the power switches accomplish zero-voltage switching. iLr1 and iLm are currently still rising and sending energy to the secondary side via wireless coils, where it is rectified by body diodes DB5 and DB8. Due to the fact that the secondary side resonant capacitor voltage VCr2 and the output voltage VBat are clamped to prevent the magnetising inductor Lm from

participating in the resonance, the magnetising current iLm keeps increasing linearly. When the resonant current iLr1 = 0, this working phase comes to a close.

4) OPERATING STAGE 2 ($t_3 < t \leq t_4$)

As seen in Fig. 8, when t = t3, the resonant current iLr1 shifts from negative to 0 while power switches S1 and S4 stay in the on position. To make sure that the resonant current iLr1 and the magnetising current iLm are not equal, VGrid currently resonates through Cr1, Cr2, Lr1, and Lr2. The current difference is then sent through the wireless coils to send energy to the secondary side, where it is rectified by body diodes DB5 and DB8 for output.It should be noted that the magnetising current iLm keeps increasing linearly and that the magnetising inductance Lm does not contribute to the resonance since it is impacted by the secondary side resonant capacitor voltage VCr2 and the output voltage VBat clamping. Given that the voltage across Cr1 is rising, the slope of iLr1 steadily falls. When the magnetising current iLm = 0, this working stage comes to a close.

C. ANALYSIS OF VOLTAGE GAIN CHARACTERISTICS

1) DERIVATION OF VOLTAGE GAIN IN FORWARD CHARGING MODE

The Fundamental Harmonic Approximation (FHA) is a commonly used technique for analysing analogous models in order to analyse the resonant circuit. An AC equivalent circuit model based on the FHA analysis approach is explained in order to better understand the design of bidirectional symmetrical resonant circuits and to determine the link between voltage gain and switching frequency. This is the AC comparable model for the forward charging mode, as seen in Fig. 11. The loosely coupled inductor's corresponding model is comparable to that of a traditional transformer.

The mathematical program Mathcad is used to demonstrate the voltage gain characteristic curves from Figures 13 to 16 in order to aid in the design of the circuit and the analysis of its properties for forward charging mode. Its features are explained, and the impact of various resonant factors on the gain curves is examined.The forward charging mode includes the following details.To make the derivation easier, an illustration of the resonant characteristic curve is provided. The fundamental magnitude of the square wave voltage produced by the primary-side switches is denoted by vin_FHA. The basic voltage magnitude across Req is denoted by veq. Clearly indicated are the primary-side resonant inductor Lr1, the primary-side resonant capacitor Cr1, and the magnetising inductor Lmar.The corresponding resonant inductor, L′ r2, and the analogous resonant capacitor, C′ r2.The secondary side reflects both of them.From the battery terminal to the primary side, the corresponding load need is shown.Equation (1) conveys the expression of requirements.

$$R_{eq} = \frac{8N^2}{\pi^2} \cdot \frac{V_{bat}}{I_{bat}} = \frac{8N^2}{\pi^2} R_{bat} \qquad (1)$$

N is the loosely coupled inductor's turns ratio in this equation, and Rbat is the battery load's equivalent impedance (Vbat/Ibat). Anode voltage, vx, is established for voltage division relationship between the input and output with regard to vx in order to determine the gain relationship between the output and input of the AC equivalent circuit. These are displayed in equations (2) to (3) with s-domain formation.

$$v_x(s) = v_{in\_FHA}(s) \cdot \frac{Z_2(s)}{Z_1(s)} \qquad (2)$$

$$v_{eq}(s) = v_x(s) \cdot \frac{Z_4(s)}{Z_3(s)} \qquad (3)$$

where the equivalent impedances from the Z1, Z2, Z3, and Z4 terminals to the outputside are represented by Z1(s), Z2(s), Z3(s), and Z4(s), which are given in equations (4) to (7).

$$Z_1(s) = sL_{r1} + \frac{1}{sC_{r1}} + Z_2(s) \qquad (4)$$

$$Z_2(s) = \frac{sL_m \cdot (sL_{r2}' + \frac{1}{sC_{r2}'} + R_{eq})}{sL_m + sL_{r2}' + \frac{1}{sC_{r2}'} + R_{eq}} \qquad (5)$$

$$Z_3(s) = sL_{r2}' + \frac{1}{sC_{r2}'} + R_{eq} \qquad (6)$$

$$Z_4(s) = R_{eq} \qquad (7)$$

When the converter is operating in the forward charging mode, the forward gain Mvr_forward may be obtained from the AC equivalent circuit by combining equations (4) to (7). Equation (8) expresses this relationship.

$$M_{vr\_forward}(s) = \frac{v_{eq}(s)}{v_{in\_FHA}(s)} = \frac{v_x(s)}{v_{in\_FHA}(s)} \cdot \frac{v_{eq}(s)}{v_x(s)} = \frac{Z_2(s)}{Z_1(s)} \cdot \frac{Z_4(s)}{Z_3(s)}$$

$$= \frac{sL_m//(sL_{r2}{}' + \frac{1}{sC_{r2}{}'} + R_{eq})}{sL_{r1} + \frac{1}{sC_{r1}} + [sL_m//(sL_{r2}{}' + \frac{1}{sC_{r2}{}'} + R_{eq})]} \cdot \frac{R_{eq}}{sL_{r2}{}' + \frac{1}{sC_{r2}{}'} + R_{eq}} \quad (8)$$

Since Lr2 ′ and Cr2 ′ are reflected from the secondary-side, the turns ratio, N, must be taken into account. These are described as follows:

$$L_{r2}{}' = N^2 L_{r2} \quad (9)$$

$$C_{r2}{}' = \frac{1}{N^2} C_{r2} \quad (10)$$

Table 1 summarises the parameters in order to simplify the mathematical formulas of the characteristics gain curves.Equation (11), which is displayed at the bottom of the next page, simplifies the voltage gain in forward charging mode by inserting the values in Table 1 into equation (8). This formula illustrates the connection between switching frequency, resonant frequency, quality factor, and resonant components.

$$M_{vr\_forward}(f_{n1\_f}) = \frac{1}{\sqrt{\left[1 + \frac{1}{k_1} - \frac{1}{k_1 (f_{n1\_f})^2}\right]^2 + q_1^2 \left[\left(1 + m_1 + \frac{m_1}{k_1}\right) f_{n1\_f} - \frac{\left(1 + \frac{1}{g_1} + \frac{1}{k_1 g_1}\right)}{f_{n1\_f}} + \frac{\left(\frac{1}{k_1 g_1}\right)}{(f_{n1\_f})^3}\right]^2}} \quad (11)$$

2) DERIVATION OF VOLTAGE GAIN IN REVERSE DISCHARIGNG MODE

Asymmetrical resonant networks make up the circuit design. The analytical techniques and procedures for the reversed charging mode are therefore the same as those for the forward charging mode; the AC equivalent model, which is displayed in Fig.12Vbat_FHArep, represents the basic magnitude of squarewave voltage produced by the secondary-side switches.Veq′ stands for the fundamental magnitude of squarewave voltage that is affected by the loosely coupled inductor and resonant components. The symbols Cr2 and Lr2 stand for the comparable resonant components on the secondary side.The primary-side resonant components are represented by the notation Cr1 ′ and Lr1 ′, respectively. On the main side, the magnetising inductor reflects Lm′.Equation (12) can be used to describe the equivalent loadReq′.

$$R'_{eq} = \frac{\frac{8}{\pi^2} \cdot \frac{V_{Grid}}{I_{Grid}}}{N^2} = \frac{\frac{8}{\pi^2} \cdot R_{Grid}}{N^2} \quad (12)$$

According to equation (12), the gridport's equivalent load is RGrid (VGrid/IGrid). Once more, the vx′ nodal voltage division is used to determine the gain connection between the output and input from the AC equivalent circuit.Equation (13) to (14) illustrates the connection between the input and output with regard to vx′ utilising this voltage ageing division.

$$v_x{}'(s) = v_{bat\_FHA}(s) \cdot \frac{Z_6(s)}{Z_5(s)} \quad (13)$$

$$v_{eq}{}'(s) = v_x{}'(s) \cdot \frac{Z_8(s)}{Z_7(s)} \quad (14)$$

With blue arrows in Fig. 12, Z5(s), Z6(s), Z7(s), and Z8(s) stand for the equivalent impedances of Z5, Z6, Z7, and Z8 terminals to the outputside. The expressions are also displayed in equations (15) to (18).

$$Z_5(s) = sL_{r2} + \frac{1}{sC_{r2}} + Z_6(s) \quad (15)$$

$$Z_6(s) = \frac{sL_{m'} \cdot (sL_{r1'} + \frac{1}{sC_{r1'}} + R_{eq'})}{sL_{m'} + sL_{r1'} + \frac{1}{sC_{r1'}} + R_{eq'}} \quad (16)$$

$$Z_7(s) = sL_{r1}{}' + \frac{1}{sC_{r1}{}'} + R_{eq}{}' \quad (17)$$

$$Z_8(s) = R_{eq}{}' \quad (18)$$

Equation (19) expresses the derivation of the input/output of the AC equivalent circuit when the converter works in the reversed discharge mode by summarising equations (15) to (18).

$$M_{vr\_reverse}(s) = \frac{v_{eq}'(s)}{v_{bat\_FHA}(s)} = \frac{v_x'(s)}{v_{bat\_FHA}(s)} \cdot \frac{v_{eq}'(s)}{v_x'(s)} = \frac{Z_6(s)}{Z_5(s)} \cdot \frac{Z_8(s)}{Z_7(s)} = \frac{sL_m' // (sL_{r1}' + \frac{1}{sC_{r1}'} + R_{eq}')}{sL_{r2} + \frac{1}{sC_{r2}} + [sL_m' // (sL_{r1}' + \frac{1}{sC_{r1}'} + R_{eq}')]} \cdot \frac{R_{eq}'}{sL_{r1}' + \frac{1}{sC_{r1}'} + R_{eq}'} \quad (19)$$

Since the primary-side resonant components reflect L′ r1 and Cr1′, the turns ratio, N, must be taken into account.The following equations (20) and (21) define them. Table 2 summarises the parameters in order to simplify the mathematical formulas of the characteristics gain curves.

$$L_{r1}' = \frac{1}{N^2} L_{r1} \quad (20)$$

$$C_{r1}' = N^2 C_{r1} \quad (21)$$

The voltage gain in reversed discharging mode is simplified in equation (22) by replacing the parameters in Table 2 into equation (19), as indicated at the bottom of the next page. This formula illustrates the connection between switching frequency, resonant frequency, quality factor, and resonant components.

$$M_{vr\_reverse}(f_{n1\_r}) = \frac{1}{\sqrt{\left[1 + \frac{1}{k_2} - \frac{1}{k_2 f_{n1\_r}^2}\right]^2 + q_2^2 \left[\left(1 + m_2 + \frac{m_2}{k_2}\right) f_{n1\_D} - \frac{\left(1 + \frac{1}{k_2} + \frac{1}{k_2 m_2}\right)}{f_{n1\_r}} + \frac{\left(\frac{1}{k_2 m_2}\right)}{f_{n1\_r}^3}\right]^2}} \quad (22)$$

]

III. DESIGN PROCEDURE AND CONSIDERATION

This system establishes an isolated bidirectional symmetrical resonant converter with a rated output power of 2 kW. research to enable two-way energy transmission between battery energy storage ports and the DC grid. The standards for lithium batteries state that a battery cell's rated operating voltage is around 3.6 V, its lowest discharge voltage is 3 V, and its maximum charging voltage is 4.2 V. As a result, the battery energy storage and discharge battery [31] in the circuit has a terminal voltage between 670 and 800 V. A list of the converter's electrical specs. For the following reasons, the switching frequency in this investigation is chosen at 100 kHz: 1. The converter can reduce the inductor volume when it is run at a high switching frequency, which lowers the total size and cost of the circuit. 2. High-frequency operation makes the output voltage smoother and more stable by lowering its ripple.3. The bidirectional LLC resonant circuit structure is used by the suggested converter in this work, therefore modifying the frequency range is required to regulate the voltage gain. A more linear modulation method in the output voltage regulation range is made possible by selecting 100 kHz as the resonant frequency point.

A. DESIGN PROCEDURES

In this part, the converter's resonant parameter design and component selection are shown. To make the circuit design easier to grasp, a flowchart that details the design process is used. provides an explanation of each phase in the design process. Additionally, the following design steps are covered. (Note: the parameters for the forward charging mode are q1, k1, g1, and m1, whereas the parameters for the reverse discharging mode are q2, k2, g2, and m2).

1) STEP 1. CONSIDER THE CONVERTER SPECIFICATIONS

VGrid (Primary), IGrid (Primary), VBat (Secondary), and IBat (Secondary) are the primary elements that influence the power level and turns ratio of the wireless coils, per the specifications of this bidirectional converter in Table 3. Additionally, all power switches have smooth switching thanks to the resonant components. The charging and discharging mode design procedure will be covered in the phases that follow.

2) STEP 2. DETERMINE THE TURNS RATION OF WIRELESS COILS

After determining the converter's input and output voltages, the wireless coil turns ratio is initially computed. In order to construct the wireless coil as indicated by equation (23), the nominal voltage of the battery, 800V, is chosen as the rated output voltage of the battery energy storage port.

$$N = \frac{N_P}{N_S} = \frac{V_{Grid}}{V_{Bat}} = \frac{400V}{800V} = 0.5 \quad (23)$$

When the suggested converter is characted for a broad output voltage and the turns ratio is calculated using the above formula, achieving the soft switching function will be challenging at various output loading levels.As a result, the circuit's overall efficiency will be affected.To ensure that the suggested converter with the wireless coils in the bidirectional energy transmission may be operated with soft switching function, the turns ratio N=0.65(0.5multiplies1.3 times) must be used.

3) STEP 3. FORWARD CHARGING MODE PARAMETER DESIGN

Equations (24) and (25) are used to compute the maximum and lowest voltage gain values of the forward charging mode, and the wireless coil turns ratio of the converter is intended to be 0.65.

$$M_{vr\_\max\_for} = \frac{N \cdot V_{Bat\_max}}{V_{Grid\_min}} = \frac{0.65 \cdot 800}{400} \cong 1.31 \quad (24)$$

$$M_{vr\_\min\_for} = \frac{N \cdot V_{Bat\_min}}{V_{Grid\_max}} = \frac{0.65 \cdot 670}{400} = 1.09 \quad (25)$$

Then, parameter values of q1, k1, g1, and m1 are chosen to satisfy the forward charging mode's voltage requirements.The gain curve should be chosen while taking into account the forward charging mode's maximum and lowest gain values.In the meanwhile, the curve is made to be as single as possible to make feedback control easier.However, because q1 will be impacted by the load, the curve that conforms to each load is chosen, and the parameters k1, g1, and m1 are fixed.The design standard's maximum output load power voltage and current are 800V and 2.5A, respectively.Given that this circuit runs in two directions, the chosen resonant parameters must satisfy the bidirectional voltage regulation. However, as this technique cannot be implemented with a single designed parameter, the planned resonant parameters must be modified periodically to meet the bidirectional design criteria. Last but not least, the bidirectional voltage gain design of this circuit is displayed in Fig. 18 with q1 = 0.2, k1 = 3, g1 = 1, and m1 = 1.After figuring out the values of q1, k1, g1, and m1, the following formulas are used to get the parameters of the resonant components needed for the converter and the wireless coils.

$$R_{eq} = \frac{8N^2}{\pi^2} \cdot \frac{V_{Bat}}{I_{Bat}} = \frac{8}{\pi^2} \cdot \frac{800}{2.5} \cong 111.8\Omega \quad (26)$$

$$C_{r1} = \frac{1}{2\pi \cdot f_{r1\_f} \cdot R_{eq} \cdot q_1} = \frac{1}{2\pi \cdot 100\text{k} \cdot 111.8 \cdot 0.2} \cong 71nF \quad (27)$$

$$L_{r1} = \frac{1}{(2\pi \cdot f_{r1\_f})^2 \cdot C_{r1}} = \frac{1}{(2\pi \cdot 100\text{k})^2 \cdot 71n} \cong 35.2\mu H \quad (28)$$

$$L_{m1} = L_{r1} \cdot k_1 = 35.2\mu \cdot 3 \cong 105.6\mu H \quad (29)$$

B. DIGITAL SIGNAL CONTROLLER APPLICATION

1) CONTROL SIGNAL CONTROLLER APPLICATION

Texas Instruments' TMS320F28335 digital signal processor serves as the double conversion system's control core in this project, enabling bidirectional power regulation and system control strategy planning. The non-contact resonant converter's control system design is depicted in Fig. 23.

2) REVERSE DISCHARGING MODE CONTROL SYSTEM

The control system block of the reverse charging mode is displayed in Fig. 25.To keep the grid voltage stable, the feedback in this mode will employ the constant voltage mode. The sample value is transmitted to the ADC via the DC grid voltage Vgrid after passing through the sampling circuit. The reference voltage signal Vgrid_ref is subtracted from the sampling value. The frequency generator (FM generator) processes the DC grid voltage and sends a frequency conversion signal (PWM) to the proportional integral (PI) controller for compensation.This signal is then delivered to the main circuit in order to regulate the voltage and modify the power.This signal is then delivered to the main circuit in order to regulate the voltage and modify the power.

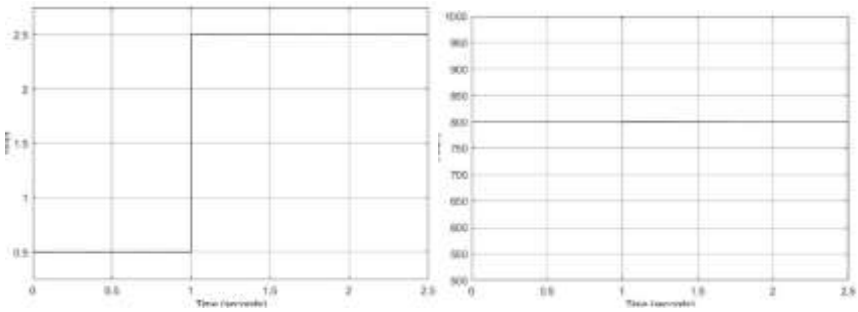

FIG 26(A)

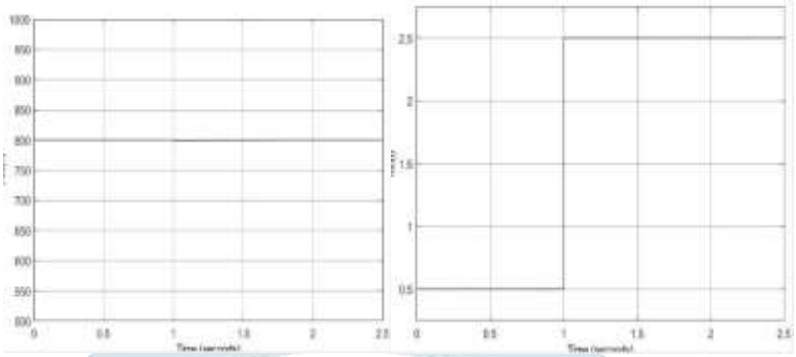

Fig26(B)

DYNAMIC LOAD VARIATION TESTING

Fig. 26 shows the load variation test of the output voltage, where *VBat*is the output voltage and *IBat*is the output current. The test of changing load current verified whether or not the output voltage can automatically adjust in response to the change of current to achieve the function of stable voltage. Figs. 26(a) and 26(b) presents that the output voltage can realize the function of constant voltage when the load current changes.

Comparison Between PI Controller and Fuzzy Logic Controller:

The PI controller operates on a mathematical model by combining proportional (P) and integral (I) components to reduce steady-state error and improve system response. It is widely used in applications requiring precise control for linear systems with stable parameters, as it is simple to design and easy to implement. However, its performance declines when the system becomes nonlinear or operates under varying conditions. PI controllers require accurate tuning of gains, and they tend to struggle with handling sudden disturbances, often leading to overshoot or sluggish recovery.

On the other hand, the Fuzzy Logic Controller (FLC) works based on linguistic, rule-based logic rather than relying on a precise system model. FLC can handle nonlinearities and uncertainties effectively, making it ideal for systems with dynamic or unpredictable behaviour. Its ability to incorporate human-like reasoning allows it to adapt to disturbances and parameter variations efficiently, ensuring better performance in complex and real-time applications. FLC offers flexibility and robustness but comes at the cost of increased design complexity and computational requirements compared to PI controllers.

In summary, PI controllers are advantageous for simple, linear systems due to their ease of implementation and cost-effectiveness, while FLCs excel in applications with nonlinear systems, disturbances, and varying parameters, providing superior adaptability and robustness.

IV. CONCLUSION

This paper proposes and implements a wide-range, non-contact isolated bidirectional symmetric resonant converter. In order to create a converter that can be used for bidirectional energy transfer, the converter enhances the conventional LLC resonant converter circuit by adding a resonant element on the secondary side and substituting power switching elements for the rectifier diode. Wide input and output functions may be realised and the overall converter efficiency increased by addressing the issues of hard switching and low output voltage gain.To replace the conventional transformer with a non-contact wireless coil that can wirelessly transfer energy to the secondary side load terminal, a loosely linked structure and an inductively coupled wireless energy transmission technology are added to the structure. Additionally, the converter offers constant voltage (CV) and constant current (CC) charging modes that are appropriate for future EV charging systems. The use of bidirectional wireless charging between a high-voltage side with an 800V electric car battery and a low-voltage side with a 400V DC grid is the main focus of the proposed study. The adaptability of wireless charging applications is greatly increased by this contribution.

REFERENCES

[1] A. S. Babokany, M. Jabbari, G. Shahgholian, and M. Mahdavian, ‘‘A review of bidirectional dual active bridge converter,’’ in Proc. 9th Int. Conf. Electr. Eng./Electron., Comput., Telecommun. Inf. Technol., May 2012, pp. 1–4.

[2] K.Tytelmaier,O.Husev,O.Veligorskyi,andR.Yershov,‘‘Areviewofnon isolated bidirectional DC–DC converters for energy storage systems,’’ in Proc. 2nd Int. Young Scientist Forum Appl. Phys. Eng. (YSF), Oct. 2016, pp. 22–28.

[3] L. Qu, X. Wang, D. Zhang, Z. Bai, and Y. Liu, ‘‘A high efficiency and low shutdown current bidirectional DC–DC CLLLC resonant converter,’’ in Proc. 22nd Int. Conf. Electr. Mach. Syst. (ICEMS), Aug. 2019, pp. 1–6, doi: 10.1109/ICEMS.2019.8922079.

[4] R. Zgheib, K. Al-Haddad, and I. Kamwa, ‘‘V2G, G2V and active filter operation of a bidirectional battery charger for electric vehicles,’’ in Proc. IEEE Int. Conf. Ind. Technol. (ICIT), Mar. 2016, pp. 1260–1265, doi: 10.1109/ICIT.2016.7474935.

[5] Z. U. Zahid, Z. M. Dalala, R. Chen, B. Chen, and J.-S. Lai, ‘‘Design of bidirectional DC–DC resonant converter for vehicle-to-grid (V2G) appli cations,’’ IEEE Trans. Transport. Electrific., vol. 1, no. 3, pp. 232–244, Oct. 2015, doi: 10.1109/TTE.2015.2476035.

[6] Y. Zhou and C. Ngai-Man Ho, ‘‘A review on microgrid architectures and control methods,’’ in Proc. IEEE 8th Int. Power Electron. Motion Control Conf., May 2016, pp. 3149–3156.

[7] W. Zhang and J. Wang, ‘‘Research on V2G control of smart microgrid,’’ in Proc. Int. Conf. Comput. Eng. Intell. Control (ICCEIC), Nov. 2020, pp. 216–219.

[8] R. G. Gago, S. F. Pinto, and J. F. Silva, ‘‘G2V and V2G electric vehicle charger for smart grids,’’ in Proc. IEEE Int. Smart Cities Conf. (ISC2), Sep. 2016, pp. 1–6, doi: 10.1109/isc2.2016.7580786.

[9] B. Zhao, X. Zhang, and J. Huang, ‘‘AI algorithm-based two-stage opti mal design methodology of high-efficiency CLLC resonant converters for the hybrid AC–DC microgrid applications,’’ IEEE Trans. Ind. Electron., vol. 66, no. 12, pp. 9756–9767, Dec. 2019.

[10] I. Aghabali, J. Bauman, P. J. Kollmeyer, Y. Wang, B. Bilgin, and A. Emadi, ‘‘800-V electric vehicle powertrains: Review and analysis of benefits, challenges, and future trends,’’ IEEE Trans. Transport. Electrific., vol. 7, no. 3, pp. 927–948, Sep. 2021.

[11] J.-W. Kim, M.-H. Park, B.-H. Lee, and J.-S. Lai, ‘‘Analysis and design of LLC converter considering output voltage regulation under no-load condition,’’ IEEE Trans. Power Electron., vol. 35, no. 1, pp. 522–534, Jan. 2020.

[12] R.-L. Lin and C.-W. Lin, ‘‘Design criteria for resonant tank of LLC DC–DC resonant converter,’’ in Proc. IECON- 36th Annu. Conf. IEEE Ind. Electron. Soc., Nov. 2010, pp. 427–432. 26681 VOLUME 12, 2024 S.-T. Wu, Y.-W. Chiu: Implementation of a Bidirectional 400–800V Wireless EV Charging System